Tunable-wavelength second harmonic generation from GaP photonic crystal cavities coupled to fiber tapers

Gary Shambat[1,*], Kelley Rivoire[1], Jesse Lu[1], Fariba Hatami[2], and Jelena Vučković[1]

[1]*Department of Electrical Engineering, Stanford University, Stanford 94305, USA*
[2]*Department of Physics, Humboldt University, D-10115, Berlin, Germany*
**gshambat@stanford.edu*

Abstract: We demonstrate up to 30 nm tuning of gallium phosphide photonic crystal cavities resonances at ~1.5 μm using a tapered optical fiber. The tuning is achieved through a combination of near-field perturbations and mechanical deformation of the membrane, both induced by the fiber probe. By exploiting this effect, we show fiber-coupled second harmonic generation with a tuning range of nearly 10 nm at the second harmonic wavelength of ~750 nm. By scaling cavity parameters, the signal could easily be shifted into other parts of the visible spectrum.

OCIS codes: (350.4238) Nanophotonics and photonic crystals; (190.4390) Nonlinear optics, integrated optics; (230.5750) Resonators; (130.3120) Integrated optics devices; (190.2620) Harmonic generation and mixing

References and Links

1. H.-G. Park, S.-H. Kim, S.-H. Kwon, Y.-G. Ju, J.-K. Yang, J.-H. Baek, S.-B. Kim, and Y.-H. Lee, "Electrically driven single-cell photonic crystal laser," Science **305**(5689), 1444–1447 (2004).
2. D. Englund, B. Ellis, E. Edwards, T. Sarmiento, J. S. Harris, D. A. B. Miller, and J. Vuckovic, "Electrically controlled modulation in a photonic crystal nanocavity," Opt. Express **17**(18), 15409–15419 (2009).
3. A. M. Armani, R. P. Kulkarni, S. E. Fraser, R. C. Flagan, and K. J. Vahala, "Label-free, single-molecule detection with optical microcavities," Science **317**(5839), 783–787 (2007).
4. D. Englund, A. Faraon, I. Fushman, N. Stoltz, P. Petroff, and J. Vucković, "Controlling cavity reflectivity with a single quantum dot," Nature **450**(7171), 857–861 (2007).
5. Y. Akahane, T. Asano, B. S. Song, and S. Noda, "High-Q photonic nanocavity in a two-dimensional photonic crystal," Nature **425**(6961), 944–947 (2003).
6. A. Faraon, and J. Vuckovic, "Local temperature control of photonic crystal devices via micron-scale electrical heaters," Appl. Phys. Lett. **95**(4), 043102 (2009).
7. D. Dalacu, S. Frederick, P. J. Poole, G. C. Aers, and R. L. Williams, "Postfabrication fine-tuning of photonic crystal microcavities in InAs/InP quantum dot membranes," Appl. Phys. Lett. **87**(15), 151107 (2005).
8. G. Le Gac, A. Rahmani, C. Seassal, E. Picard, E. Hadji, and S. Callard, "Tuning of an active photonic crystal cavity by an hybrid silica/silicon near-field probe," Opt. Express **17**(24), 21672–21679 (2009).
9. A. Faraon, D. Englund, D. Bulla, B. Luther-Davies, B. J. Eggleton, N. Stoltz, P. Petroff, and J. Vučković, "Local tuning of photonic crystal cavities using chalcogenide glasses," Appl. Phys. Lett. **92**(4), 043123 (2008).
10. M.-K. Seo, H.-G. Park, J.-K. Yang, J.-Y. Kim, S.-H. Kim, and Y.-H. Lee, "Controlled sub-nanometer tuning of photonic crystal resonator by carbonaceous nano-dots," Opt. Express **16**(13), 9829–9837 (2008).
11. G. Shambat, Y. Gong, J. Lu, S. Yerci, R. Li, L. Dal Negro, and J. Vucković, "Coupled fiber taper extraction of 1.53 microm photoluminescence from erbium doped silicon nitride photonic crystal cavities," Opt. Express **18**(6), 5964–5973 (2010).
12. J.-Y. Kim, M.-K. Kim, M.-K. Seo, S.-H. Kwon, J.-H. Shin, and Y.-H. Lee, "Two-dimensionally relocatable microfiber-coupled photonic crystal resonator," Opt. Express **17**(15), 13009–13016 (2009).
13. K. Rivoire, Z. Lin, F. Hatami, W. T. Masselink, and J. Vucković, "Second harmonic generation in gallium phosphide photonic crystal nanocavities with ultralow continuous wave pump power," Opt. Express **17**(25), 22609–22615 (2009).
14. T. A. Birks, and Y. W. Li, "The Shape of Fiber Tapers," J. Lightwave Technol. **10**(4), 432–438 (1992).
15. K. Rivoire, A. Faraon, and J. Vuckovic, "Gallium phosphide photonic crystal nanocavities in the visible," Appl. Phys. Lett. **93**(6), 063103 (2008).
16. M. Kim, J. Yang, Y. Lee, and I. Hwang, "Influence of etching slope on two-dimensional photonic crystal slab resonators," J. Korean Phys. Soc. **50**(4), 1027–1031 (2007).
17. C. W. Wong, P. T. Rakich, S. G. Johnson, M. Qi, H. I. Smith, E. P. Ippen, L. C. Kimerling, Y. Jeon, G. Barbastathis, and S.-G. Kim, "Strain-tunable silicon photonic band gap microcavities in optical waveguides," Appl. Phys. Lett. **84**(8), 1242–1244 (2004).

#125594 - $15.00 USD Received 17 Mar 2010; revised 11 May 2010; accepted 18 May 2010; published 25 May 2010

18. T. Zander, A. Herklotz, S. Kiravittaya, M. Benyoucef, F. Ding, P. Atkinson, S. Kumar, J. D. Plumhof, K. Dörr, A. Rastelli, and O. G. Schmidt, "Epitaxial quantum dots in stretchable optical microcavities," Opt. Express **17**(25), 22452–22461 (2009).
19. E. G. Spencer, P. V. Lenzo, and A. A. Ballman, "Dielectric materials for electrooptic, elastooptic, and ultrasonic device applications," Proc. IEEE **55**(12), 2074–2108 (1967).
20. R. W. Dixon, "Photoelastic properties of selected materials and their relevance for applications to acoustic light modulators and scanners," J. Appl. Phys. **38**(13), 5149–5153 (1967).
21. I. Fushman, E. Waks, D. Englund, N. Stoltz, P. Petroff, and J. Vuckovic, "Ultrafast nonlinear optical tuning of photonic crystal cavities," Appl. Phys. Lett. **90**(9), 091118 (2007).
22. H. Altug, and J. Vučković, "Polarization control and sensing with two-dimensional coupled photonic crystal microcavity arrays," Opt. Lett. **30**(9), 982–984 (2005).
23. C. Manolatou, M. J. Khan, S. Fan, P. R. Villeneuve, H. A. Haus, and J. D. Joannopoulos, "Coupling of modes analysis of resonant channel add–drop filters," IEEE J. Quantum Electron. **35**(9), 1322–1331 (1999).
24. M. V. Dutt, L. Childress, L. Jiang, E. Togan, J. Maze, F. Jelezko, A. S. Zibrov, P. R. Hemmer, and M. D. Lukin, "Quantum register based on individual electronic and nuclear spin qubits in diamond," Science **316**(5829), 1312–1316 (2007).
25. K. Rivoire, A. Kinkhabwala, F. Hatami, W. T. Masselink, Y. Avlasevich, L. Mullen, W. E. Moerner, and J. Vuckovic, "Lithographic positioning of fluorescent molecules on high-Q photonic crystal cavities," Appl. Phys. Lett. **95**(12), 123113 (2009).

1. Introduction

Nanophotonic cavities enhance light-matter interaction and have found many interesting uses in devices such as lasers [1], modulators [2], biosensors [3], as well as in fundamental experiments employing single quantum dots [4]. Photonic crystal (PC) cavities have been particularly popular due to their small mode volumes and high quality factors [5]. However, since nanofabrication techniques frequently produce cavities at wavelengths different than their intended designs, many attempts have been made to tune cavities post-processing. Mechanisms of both reversible and irreversible tuning that have been developed include local temperature control by Ohmic heaters [6], chemical etching [7], near-field tip perturbation [8], photosensitive material illumination [9], carbon dot deposition [10], and fiber taper probing [11,12]. Most tuning mechanisms provide a small resonance shift of only a few nanometers and are geared toward spectrally aligning cavities with quantum dots. On the other hand large resonance shifts of light-emitting cavities may prove as useful sources of tunable visible or IR light.

Here we report the broad tuning of a photonic crystal cavity using a fiber taper probe. In past studies, fiber taper tuning was limited to a few nanometers because the cavity modes were tightly confined inside the photonic crystal membrane, minimizing the effects of the silica fiber [11]. In this study, we fabricate our structures in an optically thin membrane to increase the proximity effect of the fiber taper. Additionally, fiber-induced deformation of the thin membranes increases the cavity resonance shift. We use these effects to show that the second harmonic (generated by cavity enhanced process [13]) signal generated can be tuned by 10 nm, half the cavity tuning range.

2. Fabrication

2.1 Taper fabrication

Fiber tapers were fabricated in the same way as in our earlier work [11], using a flame brushing procedure [14] in which a standard single mode communication fiber is simultaneously heated by a torch and pulled outward by motorized stages. The pull length was kept to a few mm to maintain the mechanical stability of the taper and to provide a high enough tension to drag the taper along the sample surface. Taper diameters were approximately 1 μm to ensure single-mode behavior.

2.2 PC cavity fabrication

Samples were grown by gas-source molecular beam epitaxy on a (100)-oriented GaP wafer. A 160 nm thick GaP membrane was grown on top of a 1 μm thick sacrificial AlGaP layer. Structures were fabricated with e-beam lithography and etching, as described in [15]. The photonic crystal cavities are three hole linear defects (L3 cavities) resonant around 1550 nm

#125594 - $15.00 USD Received 17 Mar 2010; revised 11 May 2010; accepted 18 May 2010; published 25 May 2010

wavelength [5] with lattice constant a = 500 - 560 nm, and hole radius r/a ≈0.2 – 0.25. The on-axis outer holes are shifted by 0.15a in order to improve the intrinsic Q of the cavity. Figure 1(a) shows an SEM picture of a tested cavity. After fabrication, the PC membranes were clearly seen to exhibit bowing as was evidenced by a circular ring in the undercut region of the GaP layer [Fig. 1(b)].

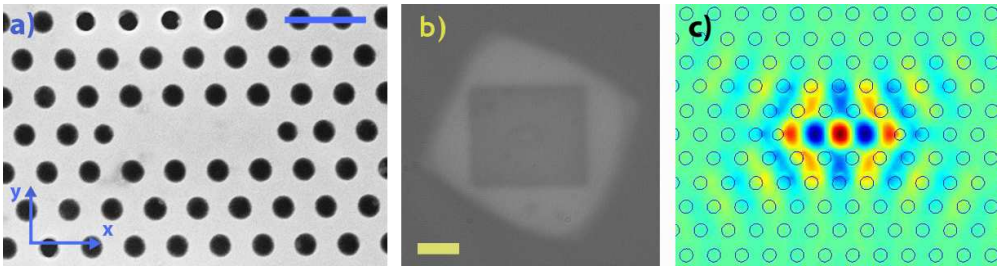

Fig. 1. (a) SEM image of a fabricated photonic crystal cavity in gallium phosphide. (b) Optical image of the same PC cavity. The central white strip is the linear cavity defect. (c) FDTD simulation profile of the dominant E_y component of the fundamental cavity resonance. The scale bars for (a) and (b) are 1 μm and 3 μm, respectively.

3. Modeling

Finite-difference time domain (FDTD) simulations were performed to determine the shift in the cavity resonance frequency produced by the fiber, both from perturbation of the cavity field and mechanical deformation of the structure. It is assumed that these two effects can be decoupled and hence can be independently analyzed in simulation. We first model the GaP cavity without any perturbation as a t = 160 nm thick slab of refractive index n = 3.1 with lattice constant a = 530 nm and hole radius r = 125 nm. The fundamental mode [Fig. 1(c)] has wavelength 1581 nm and quality factor of about 16,000.

The effect of the cavity field perturbation by a silica fiber taper, modeled as a cylinder of refractive index n = 1.45 covering the entire length of the photonic crystal membrane, is determined by simulating the cavity resonance and Q factor as the taper is scanned along the y-axis. The cavity resonance wavelength increases linearly as the taper offset, d, is decreased; on the cavity axis (d = 0), the cavity resonance is redshifted by 16 nm from the intrinsic value [Fig. 2(a)]. This value is much larger than previously observed taper-induced redshifts [11] because the cavity membrane is thin, and thus the field has a long evanescent tail in the direction perpendicular to the membrane. The effective index increase of the cavity is enhanced by the greater overlap of the cavity field with the silica material in the taper. To illustrate this effect, additional simulations with slabs thicker than 250 nm exhibited shifts of ~3 nm or less.

Interestingly, Fig. 2(b) demonstrates that there is not a monotonic relationship between taper offset and cavity total Q (Q_{tot}), but rather there appear to be points of enhanced coupling to the fiber (lower fiber Q, Q_f) at specific offsets. This is due to the fact that the cavity contains multiple polarization components with different parities and spatial patterns [e.g., see Fig. 1(c)] which couple with different strengths to the fiber depending on the taper lateral offset. Coincidentally, these points correspond to reduction of the in-plane Q ($Q_{||}$) and lossy coupling into leaky TM modes [11,16]. The maximum coupling efficiency at an offset of ~400 nm is estimated as $\eta_F = Q_{tot}/Q_f = 0.75$, which is determined by taking the integrated flux through the fiber facets and comparing to the total loss.

#125594 - $15.00 USD Received 17 Mar 2010; revised 11 May 2010; accepted 18 May 2010; published 25 May 2010

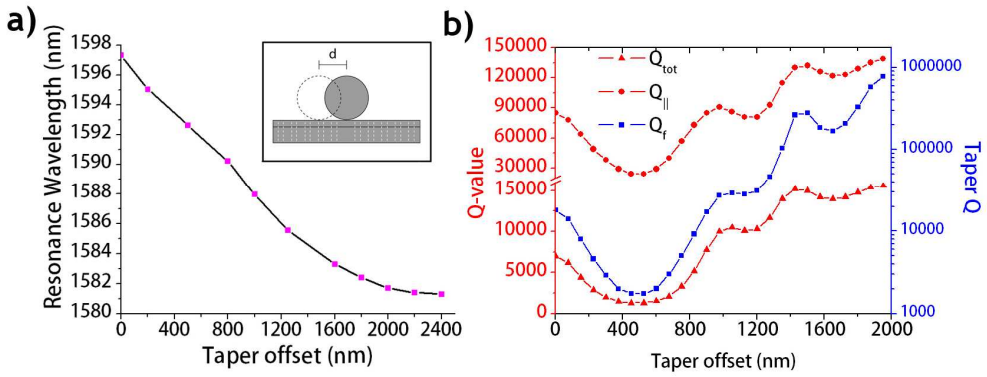

Fig. 2. (a) FDTD simulated behavior of cavity resonance as the fiber taper is displaced away from the cavity in the y-direction [see Fig. 1(a)] showing a wavelength shift from around 1597 nm to 1581 nm. The zero offset corresponds to the taper aligned with the cavity axis. (b) Simulated total Q_{tot}, in-plane $Q_{||}$, and fiber Q_f cavity quality factors as a function of taper offset. Coupling to the fiber is strongest for a 0.4 μm offset.

Physical deformation of the PC membrane creates additional redshifts due to strain-induced elongation and the photoelastic effect [17,18]. Since the PC membrane is very thin, the force of a fiber taper in contact with its surface can enhance the bowing of the membrane. From geometrical considerations, the membrane can elongate by roughly 2% before it touches the GaP substrate below the undercut region. This elongation is an upper limit since if the PC membrane were to touch the substrate, cavity confinement would be lost and the resonance would disappear. FDTD simulations show that if the PC membrane is within 300 nm of the GaP substrate, the cavity Q drops significantly. Therefore a realistic maximum for the membrane strain is ~1%.

Strain was modeled in FDTD as a uniform extension of both the lattice periodicity and the hole radius since the fiber taper contacts the cavity over a small region and therefore presses down on the membrane at a central contact point. Simulations indicate that for a 1% elongation, the cavity resonance shifts by 11 nm, with a linear relation between shift and elongation for other strain values. It should be noted that the curvature of the PC membrane itself produces no observable resonance shift in FDTD for the geometrically constrained bowing radius of curvature.

A final contribution to the resonance redshift is expected from the strain-induced refractive index increase of the semiconductor material. Qualitatively, as the membrane expands, the electronic band gap decreases, increasing the absorption and also the refractive index due to the Kramers-Kronig relations. This behavior is often modeled as a linear photoelastic effect given by (1):

$$\Delta n = -\frac{1}{2} n^3 p\ \varepsilon \qquad (1)$$

where ε is the applied strain, p is the photoelastic coefficient, n is the refractive index, and Δn is the change in refractive index [19]. Each of these constants is a tensor reflecting the appropriate crystal axes. However, here we take an average value for p in order to get an approximate average index increase and assume isotropic strain. For a strain of $\varepsilon = 0.01$, and using an average value of $p = -0.11$ for GaP [20], we calculate a refractive index change of $\Delta n \approx 0.016$, corresponding to a 7 nm redshift of the cavity resonance, which is in good agreement with the frequency-refractive index relation in [21].

All together, the three effects of fiber taper perturbation of the cavity field, physical elongation of the PC membrane, and photoelastic refractive increase of GaP sum together to produce an expected redshift of over 30 nm.

#125594 - $15.00 USD Received 17 Mar 2010; revised 11 May 2010; accepted 18 May 2010; published 25 May 2010

4. Experiment

4.1 Cavity tuning

Fabricated cavities were first characterized by free space cross-polarized reflectivity with a tungsten halogen lamp [22] to measure the intrinsic quality factor and resonance wavelength. Figure 3 shows a reflection spectrum from the cavity in Fig. 1(a), with the initial resonance wavelength of 1559 nm and the intrinsic Q factor (Q_0) equal to 3500.

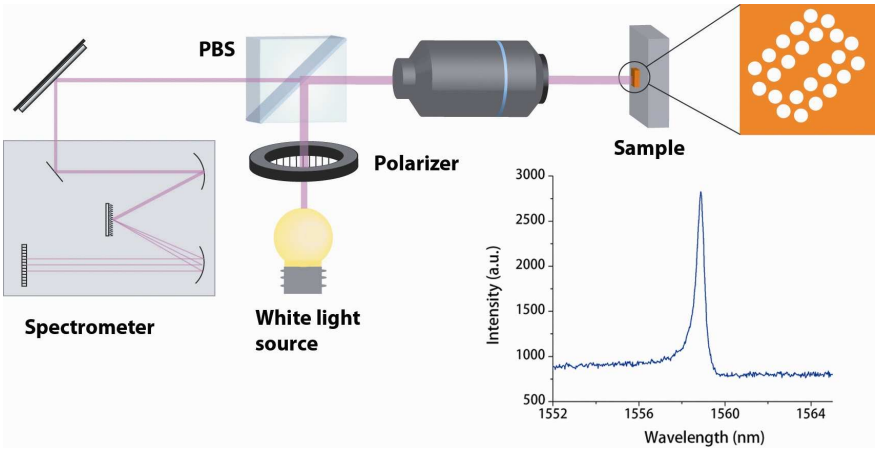

Fig. 3. Experimental setup for performing free space reflectivity measurement and results. Broadband IR light from a halogen lamp is linearly polarized and sent to the sample through a polarizing beam splitter. Cavity coupled light is reflected off the sample and is allowed to pass through the beam splitter into a spectrometer where it is detected. The spectrum shows the resulting fundamental mode reflectivity spectrum at 1559 nm.

Fiber taper-coupled transmission measurements were performed to study the tuning behavior of the cavity. Fabricated tapers were mounted and aligned as shown in Fig. 4(a), 4(b) and as described in [11]. A broadband IR source (Agilent 83437a) was coupled into the fiber, polarized, and its polarization rotated to match the cavity TE polarization. The output transmission signal was monitored with an Optical Spectrum Analyzer (OSA).

The fiber taper was first positioned at an offset of d = 2-3 μm and brought into contact with the PC surface. Initially this caused no change in the transmission spectrum except a slight scattering loss. Tension was then applied in a direction perpendicular to the cavity main axis (in the y-direction) and the fiber taper began to drag towards the cavity axis. When the taper reached an offset of ~1.5 μm, an initial coupling dip appeared at 1560 nm [Fig. 4(c)]. This signifies weak coupling and a nearly zero resonance shift since the taper was far away. As the taper was brought closer to the cavity, the cavity resonance spectrum red-shifted progressively until a maximum of 1590 nm was reached for a zero offset (i.e., taper aligned with the cavity axis). The coupling depth follows the qualitative behavior of Fig. 2(b), which predicts maximal coupling for a 0.4 μm laterally offset taper. Also in agreement with theory is the magnitude of the total redshift which was 30 nm. In the experiment, the tensioned taper presses down on the PC membrane as it is dragged along the surface. This effect could be observed while monitoring the microscope image. Therefore, all the fiber- and strain-induced effects should be taking place for the maximum redshift attained.

#125594 - $15.00 USD Received 17 Mar 2010; revised 11 May 2010; accepted 18 May 2010; published 25 May 2010

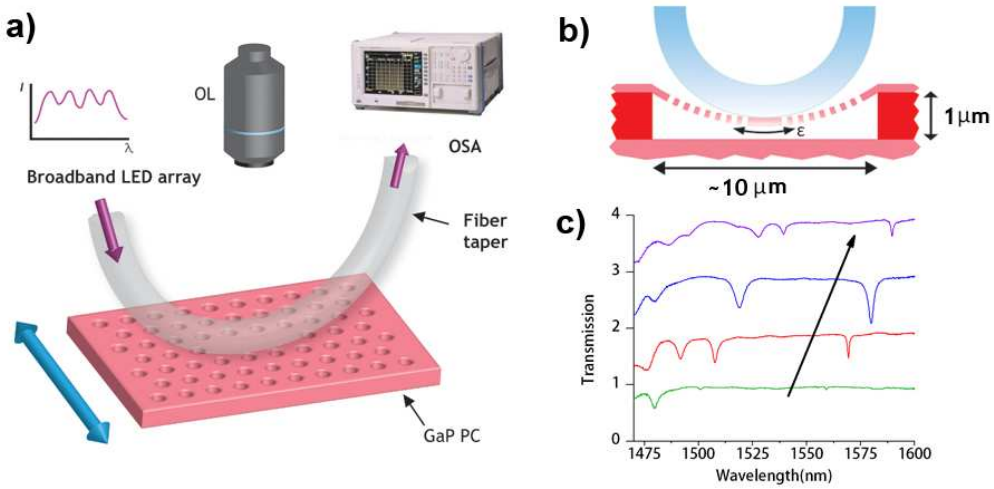

Fig. 4. (a) Setup of fiber-coupled transmission experiment. Broadband IR signal is sent through a fiber aligned along the cavity axis [x-direction in Fig. 1(a)] and the normalized transmission spectrum is measured. The blue double-arrow indicates the direction of taper scanning [y direction in Fig. 1(a)] and OL is objective lens. (b) Cross-section schematic of the taper-induced bowing effect. The pink color indicates the GaP membrane and substrate while the red indicates the remaining sacrificial AlGaP layer. The approximate dimensions are shown and the strain, ε, is noted. (c) Transmission spectra for the cavity with decreasing taper offsets in the direction of the black arrow. Spectra are vertically offset by 1 for clarity.

A close-up of the fundamental resonance tuning can be seen in Fig. 5, which plots many intermediate points between the wavelength limits. The data show the same results from before but with finer resolution. The measured Q values for the largest taper offset, largest coupling depth, and zero offset taper are 2700, 520, and 1370, respectively. In order to decouple the two effects of taper redshift versus strain redshift, we repeat the transmission experiment by slowly lowering the taper over the central axis of the cavity while monitoring the cavity resonance. When the taper-cavity gap is below ~1 μm, the initial cavity resonance appears near the intrinsic value due to weak loading. As the taper is slowly lowered the cavity resonance monotonically shifts to longer wavelengths until a maximum shift of ~17 nm is obtained at contact. Since the taper now gently rests on the surface, strain effects are minimized and the cavity resonance is redshifted because of the higher effective index of the cavity mode. From this point, the taper was tensioned while still in contact with the cavity, enhancing the visible bowing of the membrane and causing an additional 13 nm of shift. During tensioning, the contact area of the taper to cavity was unchanged and the only noticeable difference was an increase in the bowing of the membrane. Therefore we conclude that the fiber taper and strain effects sum together to produce a large tuning range for the cavity.

#125594 - $15.00 USD Received 17 Mar 2010; revised 11 May 2010; accepted 18 May 2010; published 25 May 2010

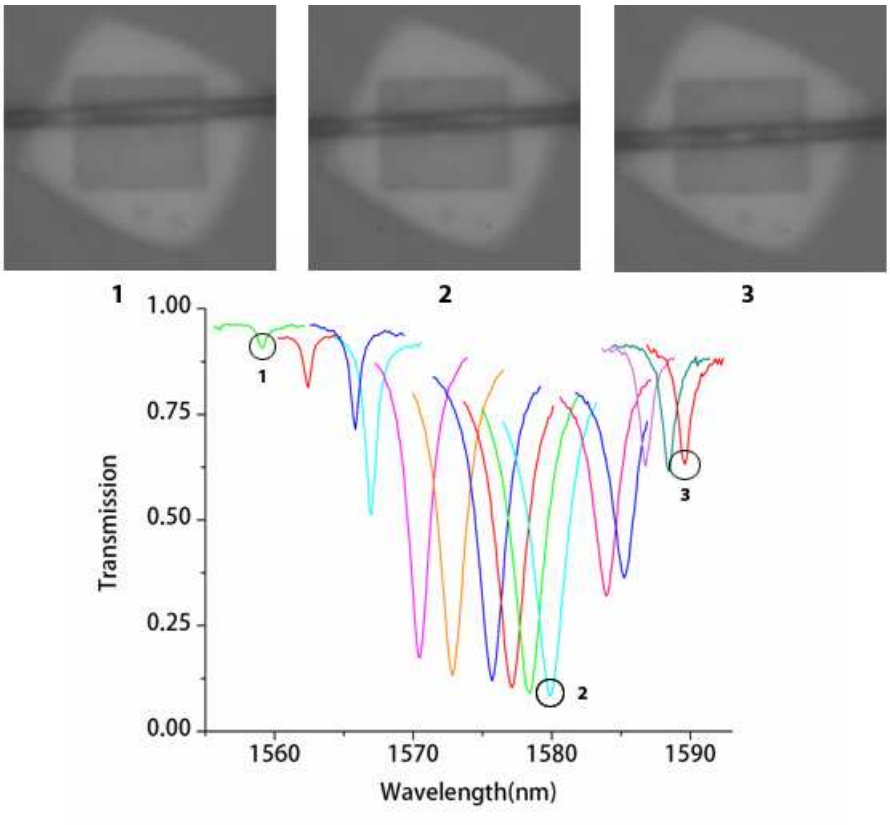

Fig. 5. Tuning of the fundamental cavity mode resonance by scanning a fiber taper from large offset in the y-direction (label 1) to zero offset (label 3). An intermediate point is also shown for label 2, where the transmission coupling is maximum.

5. Tunable second harmonic generation

We now show that the ability to tune a resonance in a PC cavity translates into a large tuning range for the second harmonic generated (SHG) in the cavity. Gallium phosphide has a large second order nonlinearity and previous experiments have shown that the SHG signal from a PC cavity embedded in GaP can be greatly enhanced by the cavity [13]. For this experiment a different cavity with tuning range of only ~20 nm at 1550 nm was used to accommodate the tuning range of the pump laser. The fiber taper was first coupled to a cavity while monitoring the broadband transmission spectrum. The input to the fiber was then switched to a tunable infrared laser that was then scanned through the cavity resonance. As this was done, SHG signal was both collected at the output of the second arm of the fiber taper and seen optically on a CCD camera (Fig. 6). The scanned output profile matches the expected Lorentzian-squared curve as seen by the fit of the data with a Q of 2200. The second harmonic generation and collection can be understood as follows: pump light from the laser first couples into the cavity TE mode from the fiber taper, then circulating pump light is frequency doubled and coupled to a TM-like Bloch mode of the PC, finally the TM Bloch mode couples back into the taper and is detected at the fiber output. Even though the TM mode is delocalized over the full PC membrane, there is still finite field overlap between it and the fundamental TM fiber mode such that coupling back into the fiber will take place.

#125594 - $15.00 USD Received 17 Mar 2010; revised 11 May 2010; accepted 18 May 2010; published 25 May 2010

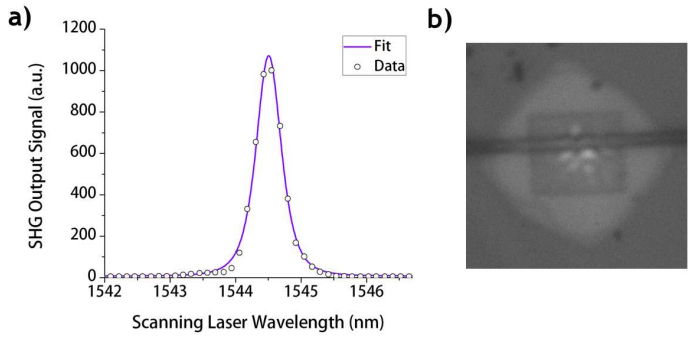

Fig. 6. (a) Second harmonic signal (around 772 nm) collected from the fiber as a pump laser is scanned through the cavity resonance. (b) Visible SHG signal seen from an overhead CCD. The delocalized nature of the propagating TM Bloch mode can be seen from the scattered light.

Tuning of the SHG signal is performed by repeating the above process for several taper positions. At each new cavity wavelength, the pump laser was adjusted to match the resonance. Figure 7 shows a plot of five different SHG signals and a few matching transmission profiles for resonances between 1540 nm and 1560 nm, corresponding to a second harmonic tuning range of ~10 nm.

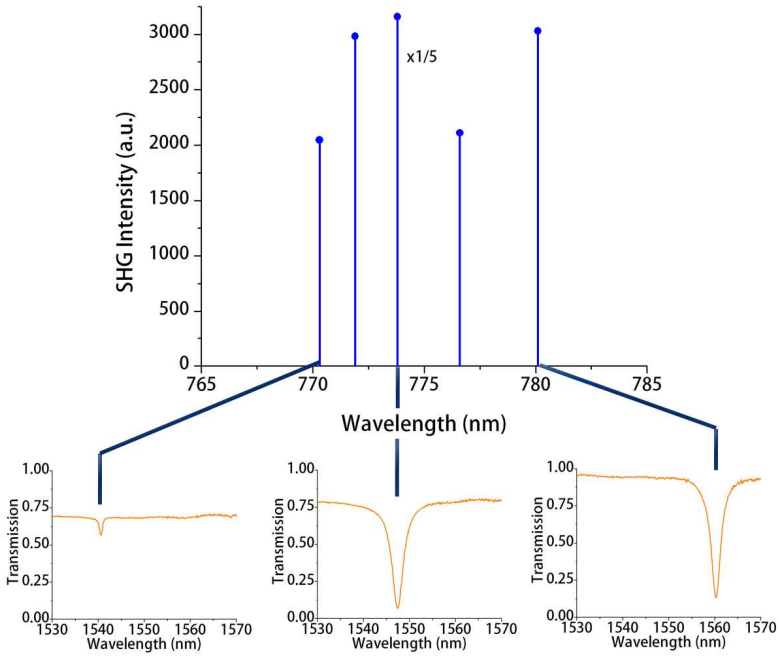

Fig. 7. Tunable second harmonic signal generated from the GaP cavity and detected through the fiber. Peaks correspond to maxima of the signal generated when the pump laser is zero detuned from the cavity resonance. The fiber taper is used to redshift the cavity resonance which translates into a change of the second harmonic output wavelength. Since the taper was aligned separately for each measurement there is some variation in the transmission spectrum background and SHG output signal strength.

The higher coupling efficiency of pump light into cavity attained via fiber pumping compared to free space pumping can produce a larger second harmonic signal. From coupled-mode theory [23], the steady-sate cavity energy for a fiber-coupled cavity is found to be $2\eta_F(1-\eta_F)P_{in}Q_0/\omega_0$, where η_F is the fiber coupling efficiency ($\eta_F = Q_{tot}/Q_f$ as above), P_{in} is the input pump power, Q_0 is the intrinsic cavity Q, and ω_0 is the cavity frequency. For free space

#125594 - $15.00 USD Received 17 Mar 2010; revised 11 May 2010; accepted 18 May 2010; published 25 May 2010

pumping the steady-state cavity energy for a cavity without a fiber is given by $2\eta_{FS}P_{in}Q_0/\omega_0$ where η_{FS} is the free space coupling efficiency of focused pump light into the cavity. A typical value of η_{FS} for this type of cavity is 5% [13] and is limited by the spatial mode matching of the pump beam and cavity. As the second harmonic generated is proportional to the cavity energy squared, the fiber-coupled cavity can produce a signal up to 25 times greater than the free space pumped cavity for $\eta_{FS} = 0.05$.

6. Conclusion

We have both theoretically and experimentally demonstrated a 30 nm tuning range of GaP photonic crystal cavities fabricated for 1550 nm operation. In these thin PC membranes, the cavity mode evanescent tail extends out farther into the air cladding and is strongly affected by the fiber taper, which introduces a large effective index perturbation. The thin membrane also allows for enhanced taper-induced bowing effects, which deform (stretch) the cavity structure and increases the material refractive index by the photoeleastic effect. By taking advantage of the $\chi^{(2)}$ nonlinearity in gallium phosphide along with the large tuning effect of the taper, we also demonstrate second harmonic generation that is tunable over a 10 nm range. By scaling cavity parameters, the wavelength of the tunable second harmonic can be shifted farther into the visible since the bandgap of GaP is at 555 nm. Such a source could find applications in quantum optics spectroscopy [24], biosensing, and imaging of molecules [25].

Acknowledgements

The authors acknowledge the support of the Interconnect Focus Center, one of six research centers funded under the Focus Center Research Program (FCRP), a Semiconductor Research Corporation entity. Gary Shambat would like to thank the NSF GRF for support and Kelley Rivoire would like to thank the Stanford Graduate Fellowship for support. The fabrication has been performed in the Stanford Nanofabrication Facilities.

#125594 - $15.00 USD Received 17 Mar 2010; revised 11 May 2010; accepted 18 May 2010; published 25 May 2010